INVESTIGATIONS OF THERMOHYDRAULIC PERFORMANCE IN HEAT EXCHANGER TUBE WITH RECTANGULAR VORTEX GENERATORS

Shiquan ZHU [1,2,]*, Longjiang LI [1,2], Zongyao HU [1,2], Tian QI [1,2], Shuang CAO [1,2], Zhenya ZHANG [1,2], Yisen PENG [1,2]

[1] School of Energy and Power Engineering, Zhengzhou University of Light Industry, Zhengzhou, 450002, China

[2] Henan International Joint Laboratory of Energy Efficient Conversion and Utilization, Zhengzhou University of Light Industry, Zhengzhou, 450002, China

[*] Corresponding author; E-mail: zhusq0701@163.com

To demonstrate the rationalization of multi-longitudinal swirls (MLSs) in heat exchanger tubes, this paper investigates the thermohydraulic performance of heat exchanger tube with rectangular vortex generator using numerical simulation. Comparative analyses of rectangular vortex generators and their different slotted structures are conducted, along with the investigation of the effect of the longitudinal pitch (P = 0.1 m, 0.2 m and 0.3 m) of the rectangular vortex generators on the thermohydraulic performance. The research reveals that the MLSs induced by the vortex generator inside the tube accelerate the exchange of cold and hot fluids, improve the field synergies of velocity vectors and temperature gradients, and enhance the heat transfer efficiency of the heat exchanger tube. The slotted structure reduces the flow resistance and lowers the degree of disturbance to the fluid, which reduces the strength of the MLSs, thus weakening the overall performance of the heat exchanger. The strength of the MLSs has a direct influence on the overall performance of the heat exchanger tube. With the increase of P, the performance evaluation criteria (PEC) of the heat exchanger tubes decreases, and the maximum PEC = 1.44 is obtained for P = 100 mm at the studied Reynolds number range.

Key words: *thermohydraulic performance*; *rectangular vortex generators*; *multi-longitudinal swirls*; *numerical simulation*

1. Introduction

Nowadays, with the progression of economic and social development, the energy demand of humans is continuously escalating. Meanwhile, natural resource reserves such as oil and coal are decreasing, making it imperative to enhance the efficiency of energy utilization. Heat exchangers play a vital role in the heating and ventilation, petroleum and chemical industries, and thus improvement in heat transfer efficiency is conducive to energy saving, emission reduction and developing green economy [1]. Therefore, enhanced heat transfer is crucial for the design of the thermal channel and has attracted the attention of many researchers. Enhanced heat transfer technology may be categorized into three categories: active, passive and compound technologies. Of these, passive technologies have received more attention in industrial applications because they do not need external energy supply, are easy to manufacture, have simple design, have high stability and are easy to maintain. In the development and application of passive enhanced heat transfer technology, the contradiction between enhanced convection heat transfer and flow resistance is the primary challenge to consider. How to improve convective heat transfer along with smaller flow resistance penalty is the key to the improvement of the overall performance of the heat exchanger. The optimal flow field structure is primarily characterized by multi-longitudinal swirls (MLSs) [2], which can achieve a good balance between enhanced convection heat transfer and flow resistance. In light of heat transfer challenges, MLSs provide a novel direction for the advancement of enhanced heat transfer.

The MLSs in the thermal channel facilitate the disruption the thermal boundary layer, promote the exchange of cold and hot fluids, and decrease the synergy angle between the temperature gradient and the temperature vector. Consequently, the MLSs reduces power consumption in the heat transfer process and improves the overall performance of the thermal channel. Ekrani *et al.* [3] examined the thermohydraulic phenomenon of the tube with delta winglet vortex generator through numerical simulation. The findings revealed that the primary mechanism responsible for enhanced heat transfer was the delta winglet induced MLSs, which destroys the boundary layer and strengthen the exchange of hot and cold fluids. Meng *et al*. [4] examined the enhanced heat transfer phenomenon of a discrete double-inclined ribs tube and revealed the enhanced heat transfer mechanism of MLSs from the field synergy perspective. The MLSs decrease the synergy angle between the temperature gradient and velocity vector, thereby enhancing fluid heat transfer. Khaboshan *et al*. [5] examined the MLSs on the thermal phenomenon in alternating elliptical tube. The findings revealed that the MLSs augment the exchange of cold and hot fluids and increase the convective heat transfer coefficient. Wang *et al.* [6] examined the thermohydraulic phenomenon of the tube with symmetrical wing. Their findings attributed the enhanced heat transfer mechanism to two primary reasons, the first is that the symmetrical wing generates MLSs, and the second is that the symmetrical wing similarities the deflector plate to guide the fluid mixing. Batule *et al.* [7] examined the thermohydraulic phenomenon of circular pipe with circular spines. The findings revealed that the curved circular spines induced MLSs in the tube, which disturbed the fluid flow and reduced the dominant thermal resistance, thereby improving the convective heat transfer. Xiao *et al.* [8] examined the turbulent heat transfer phenomenon in the tube with v-ribs. The findings revealed that the v-ribs generate the MLSs in the tube, maintaining the secondary flow intensity and enhancing heat transfer. Liu *et al.* [9] examined the thermohydraulic phenomena of a novel tube with conical strip. The conical strip generates MLSs in the novel tube, resulting in higher thermal performance with lower flow loss, thus improving the overall performance of the novel tube. Lv *et al.* [10] analyzed the thermohydraulic phenomenon of the tube with center-connected deflectors based on the principle of exergy destruction minimization. The findings revealed that the deflectors guided the fluid flow from the core flow region towards the wall region and generated MLSs in the tube, which enhances heat transfer. Ali *et al.* [11] examined the enhanced heat transfer and mixing phenomenon of the tube with flexible vortex generators. The findings revealed that the flexible vortex generators generate MLSs in the tube, which compress the velocity shear layers and improves the overall performance of the tube. The MLSs technology provides guidance for the application of enhanced heat transfer technology, guiding the design of the spoiler element with excellent performance from the mechanism, which is crucial for improving the overall performance of the thermal channel.

According to the above literature, the disturbance element generates MLSs in the thermal channel, resulting in high heat transfer capacity with relatively low pressure drop penalties. Consequently, spoiler element capable of generating MLSs have significant attention. Reasonable arrangement of the rectangular vortex generator can induce fluid generate MLSs in the thermal channel, and the current research seldom combines this with the MLSs technology. The rectangular vortex generator enables fluid to form the MLSs in the tube, reducing the flow loss and achieving larger heat transfer capacity with the lower pressure drop penalties, thus improving the overall performance of the thermal channel. Therefore, the design of a vortex generator capable of inducing MLSs for fluid in the tube is the core of this study to enhance heat transfer.

This work conducts the comparative analysis of the effect of rectangular vortex generators on thermohydraulic phenomenon of the tubes, and the effect of slotted structure on the formation of MLSs induced by vortex generators. The effects of the slotted structure on the internal flow and temperature fields, as well as the pitch of rectangular vortex generators on the intensity of MLSs, are investigated using numerical methods. This understanding aims to elucidate the heat transfer mechanism of the vortex generator and demonstrate the rationality of MLSs generation.

2. Numerical simulations

2.1. Physical model

The geometrical model of the rectangular vortex generator (A0) of the circular tube is shown in Fig. 1(a). The inner diameter of the tube is d=0.047 m and the test section length is 1 m. The vortex generators are arranged in the circumferential direction of the tube, and two adjacent vortex generators are arranged in the V-shape row, and the leading edge of the vortex generators is 0.2 m away from the entrance of the test section. The length (L), height (H) and width (W) of the vortex generators are 0.0098 m, 0.0047 m and 0.001 m, respectively. The attack angle (β) is 30°. To ensure that the test section inlet is a fully developed turbulent state during numerical calculations and that no backflow occurs at the test section outlet, the computational domain is extended upstream and downstream by 0.5 m and 0.3 m, respectively. Furthermore, to investigate the effect of the vortex generator on the generation of MLSs, three different slotted structures, A1, A2 and A3, were designed on the basis of A0, as represented in Fig. 1(b).

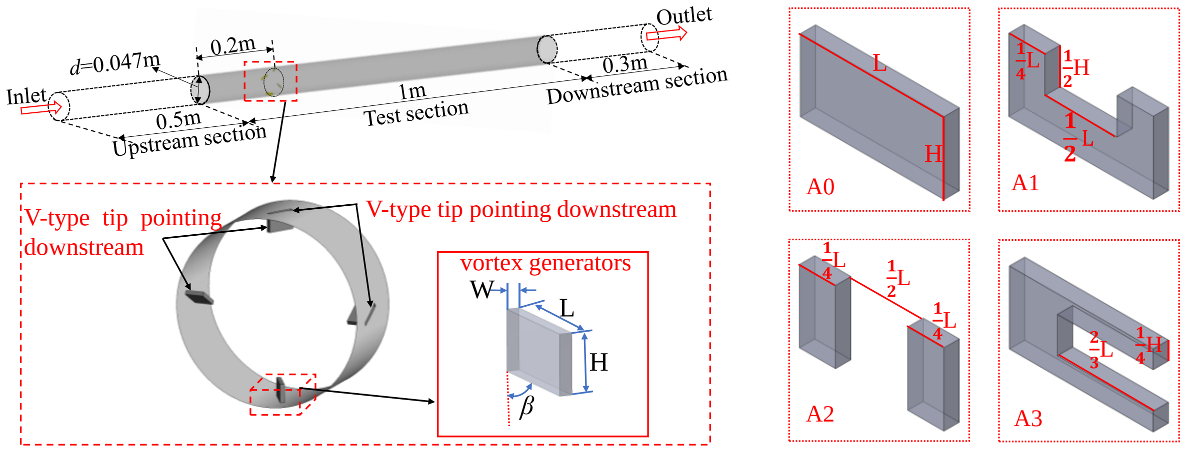

Figure 1. The geometric model: (a) Tube with vortex generator; (b) Slotted structure

2.2. Governing equations and boundary conditions

In this work, the commercial software Ansys-Fluent is employed for numerical simulation calculations. Specific assumptions are made in conjunction with the fluid flow and heat transfer conditions in the tube, which are as follows:

(1) The working medium is water, and it is incompressible steady state flow;

(2) The effect of gravity is ignored;

(3) Only heat conduction between fluids and convective heat transfer between solid and fluid are considered.

According to the above assumptions, the *SST k-ω* turbulence model is implemented, leading to the following governing equations:

Continuity equation:

$$\frac{\partial(\rho u)}{\partial x}+\frac{\partial(\rho v)}{\partial y}+\frac{\partial(\rho w)}{\partial z}=0 \tag{1}$$

Momentum equation:

$$\frac{\partial(\rho u)}{\partial t}+u\frac{\partial(\rho u)}{\partial x}+v\frac{\partial(\rho u)}{\partial y}+w\frac{\partial(\rho u)}{\partial z}=-\frac{\partial p}{\partial x}+\frac{\partial \tau_{xx}}{\partial x}+\frac{\partial \tau_{yx}}{\partial y}+\frac{\partial \tau_{zx}}{\partial z}+F_x \tag{2}$$

$$\frac{\partial(\rho v)}{\partial t}+u\frac{\partial(\rho v)}{\partial x}+v\frac{\partial(\rho v)}{\partial y}+w\frac{\partial(\rho v)}{\partial z}=-\frac{\partial p}{\partial y}+\frac{\partial \tau_{xy}}{\partial x}+\frac{\partial \tau_{yy}}{\partial y}+\frac{\partial \tau_{zy}}{\partial z}+F_y \tag{3}$$

$$\frac{\partial(\rho w)}{\partial t}+u\frac{\partial(\rho w)}{\partial x}+v\frac{\partial(\rho w)}{\partial y}+w\frac{\partial(\rho w)}{\partial z}=-\frac{\partial p}{\partial z}+\frac{\partial \tau_{xz}}{\partial x}+\frac{\partial \tau_{yz}}{\partial y}+\frac{\partial \tau_{zz}}{\partial z}+F_z \tag{4}$$

Energy equation:

$$\frac{\partial(\rho T)}{\partial t}+u\frac{\partial(\rho T)}{\partial x}+v\frac{\partial(\rho T)}{\partial y}+w\frac{\partial(\rho T)}{\partial z}=\frac{\partial}{\partial x}\left(\frac{k}{C_p}\frac{\partial T}{\partial x}\right)+\frac{\partial}{\partial y}\left(\frac{k}{C_p}\frac{\partial T}{\partial y}\right)+\frac{\partial}{\partial z}\left(\frac{k}{C_p}\frac{\partial T}{\partial z}\right)+S_T \tag{5}$$

k and ω equations:

$$\frac{\partial}{\partial t}(\rho k)+\frac{\partial}{\partial x_i}(\rho k u_i)=\frac{\partial}{\partial x_j}\left(\Gamma_k\frac{\partial k}{\partial x_j}\right)+G_k-Y_k \tag{6}$$

$$\frac{\partial}{\partial t}(\rho \omega)+\frac{\partial}{\partial x_i}(\rho \omega u_i)=\frac{\partial}{\partial x_j}\left(\Gamma_\omega\frac{\partial \omega}{\partial x_j}\right)+G_\omega-Y_\omega \tag{7}$$

where, G_k represents the generated turbulent kinetic energy, G_ω represents the generation of specific dissipation rate, Γ_k and Γ_ω represent the effective diffusion coefficients, Y_k and Y_ω represent the dissipation caused by turbulence.

Velocity inlet boundary and pressure outlet boundary are applied, the inlet velocity u_{in} is 0.2-0.6 m/s, the inlet temperature is 293 K. The wall is assumed to be no-slip boundary conditions. The uniform heat flux of 30000 W/m^2 are applied on the wall. The physical properties of water are as follows: Prandtl number Pr = 7.02, density ρ = 998.2 kg·m^{-3}, specific heat capacity C_p = 4183 J/(kg·K), thermal conductivity k = 0.6 W/(m·K), and dynamic viscosity μ = 0.001003 Pa·s.

2.3. Data processing

The reynolds number (*Re*), friction factor (*f*), heat transfer coefficient (*h*), Nusselt number (*Nu*) and performance evaluation criteria (PEC) are defined by the following equations:

$$Re=\frac{u_m D_h}{\lambda} \tag{8}$$

$$h=\frac{q}{T_w-T_m} \tag{9}$$

$$Nu=\frac{hD_h}{k} \tag{10}$$

$$f=\frac{\Delta p}{(l/d)\rho u_m^2/2} \tag{11}$$

where, u_m is the fluid flow rate; D_h is the hydraulic diameter; μ is the dynamic viscosity; q is the constant heat flux; T_w is the average temperature of the tube wall; T_m is the fluid mean temperature; k is the thermal conductivity coefficient; Δp is the pressure difference between the inlet and outlet of the test section; and l is the test section length.

To evaluate the thermohydraulic performance of the thermal channel, the performance evaluation criteria (PEC) is applied, which represents the ability to enhance heat transfer under equal pump power [9].

The defining equation is shown below:

$$\mathrm{PEC} = \frac{Nu/Nu_0}{\left(f/f_0\right)^{1/3}} \tag{12}$$

where, Nu and Nu_0, and f and f_0 represent the Nusselt numbers and the friction factors of the tube with vortex generators (in further text: enhanced tube) and smooth tube, respectively.

2.4. Grid system and grid independence validation

The Ansys-ICEM module is employed to mesh the computational domain, generating hexahedral structured grids to ensure the orthogonality and accuracy of the grid, as shown in Fig. 2. According to the boundary conditions of the model, physical parameters of the water, and turbulence model, the height of the first layer of the grid is calculated, ensuring that y ≈ 1. Grid independence verification is carried out for the rectangular vortex generator at the Re = 14000, and the results are shown in Fig. 3. The maximal deviations of Nu and f are 0.25% and 0.21%, respectively, as the number of grids is increased from 2.4 million to 3 million. This demonstrates that the grid system with about 2.4 million can ensure the accuracy requirements of the results while saving computational resources. Therefore, in the numerical simulation of this work, the same meshing method as this is employed for all the working conditions.

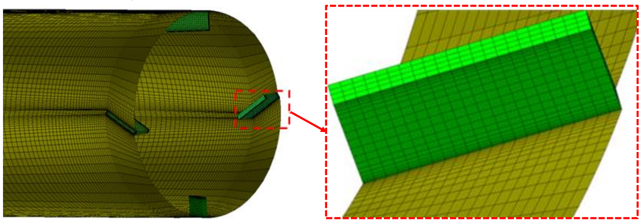

Figure 2. Grids distribution of tube wall and vortex generators

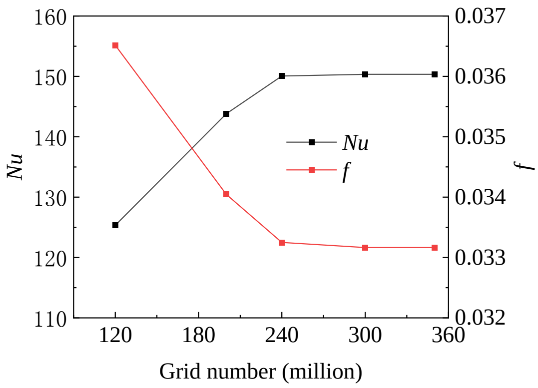

Figure 3. Grid independence verification

2.5. Model validation

To verify the accuracy of the numerical method, numerical simulations of the flow and heat transfer processes in the smooth tube is carried out and the calculated results are compared with empirical correlations. The findings are shown in Fig. 4, the maximum Nu deviation compared with Gnielinski correlation [12] and Dittus-Boelter correlation [12] is 7.04% and 7.67%, respectively; and the maximum f deviation compared with Filonenko correlation [12] and Blasius correlation [12] is 6.93% and 6.47%, respectively. Therefore, the numerical method employed in this work is presumed to be sufficiently accurate and efficient.

Gnielinski correlation:

$$Nu = \frac{(f/8)(Re-1000)Pr}{1+12.7(f/8)^{1/2}(Pr^{2/3}-1)} \tag{13}$$

Dittus-Boelter correlation:

$$Nu = 0.023Re^{0.8}Pr^{0.4} \tag{14}$$

Filonenko correlation:

$$f = (1.82\lg Re - 1.64)^{-2} \tag{15}$$

Blasius correlation:

$$f = 0.316Re^{-0.25} \tag{16}$$

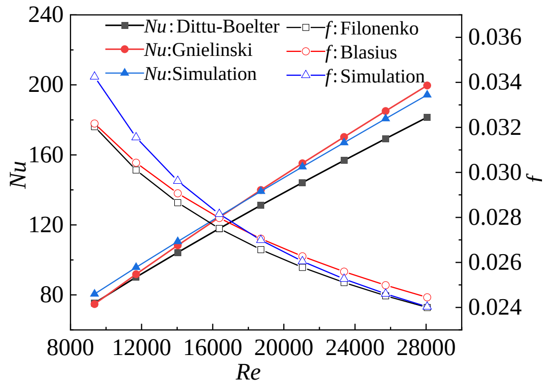

Figure 4. The numerical calculation of *Nu* and *f* compared with the empirical formulas

3. Results and discussion

3.1. Effect of rectangular vortex generators and different slotted structures on the thermohydraulic performance

3.1.1 Turbulent flow structures and thermal fields

Fig. 5 shows the streamline distribution before and after the fluid flows through vortex generators. It can be observed that the vortex generator impedes the fluid flow in the tube and changes the fluid flow path, as the fluid downstream of the vortex generator leading edge converges into the longitudinal swirls. The degree of the streamline disruption behind the vortex generator structures reflects the degree of fluid disturbance, which differs among the various slotted structures. Behind the A1 structure, it is clearly visible that part of the flow line is deflected and the flow direction is changed, which is not prominent for the A2 and A3 structures. This is due to the fact that the fluid flows through the slotted position to form the jet, which mixes with the other fluids at the rear and moves along the main flow direction. The streamlines behind the A0 structure are more intensely deflected, with the fluid streamlines exhibiting a spiral motion along the flow direction and ultimately towards the center region of the tube. Thus, the slotted structure reduces fluid stagnation while also diminishing the strength of the longitudinal swirl it generates.

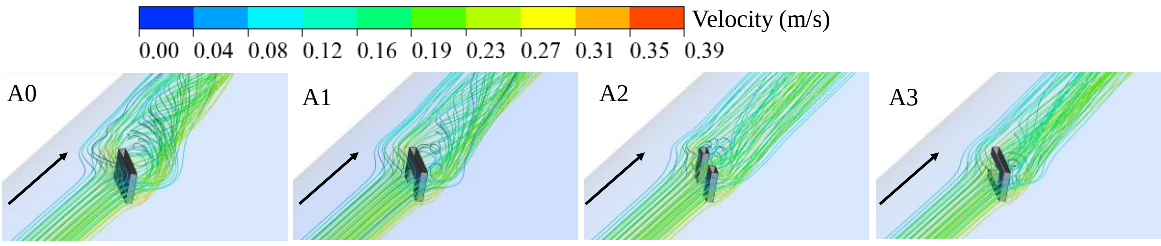

Figure 5. Local streamlines (*Re*=14000)

Fig. 6 shows the velocity vector distributions in the cross-sections Z1 and Z2 after flow through the vortex generator (*Re* = 14000). Four longitudinal swirls (two pairs of longitudinal swirls with opposite directions) are generated in the tube, which is associated with the V-type arrangement of the vortex generator. The velocity vectors distribution of the slotted structures reveals that the intensity of the vortices generated on cross-section Z1 is significantly greater than that on cross-section Z2, indicating that the intensity of the vortices decreases along the flow direction. The swirl intensity of the A1 structure is higher than that of the A2 and A3 structures, indicating that the slotted position and area significantly affect the intensity of the MLSs. The A0 structure generates the stronger swirl than the slotted structure and decays more slowly along the flow direction. Consequently, the MLSs have a more pronounced influence on the fluid in the A0 tube.

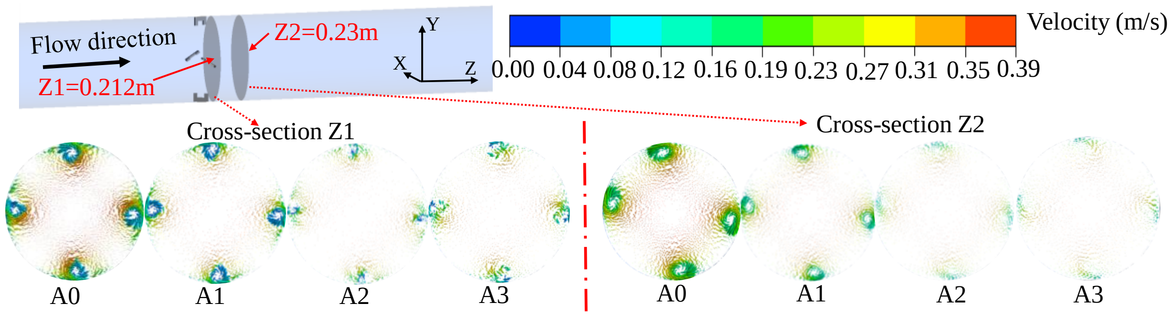

Figure 6. Velocity vector cross-section diagram (*Re* = 14000)

Fig. 7 shows the velocity and streamline distributions on cross-sections Z1 and Z2 for both the smooth tube and the enhanced tube at *Re* = 14000. The vortex generators of various configurations generate significant MLSs, with higher velocities near the center region and lower flow velocities near the wall region. As the flow path extends, the flow velocity in the center region of the tube decreases gradually. This indicates that the MLSs along the main flow direction enhance the fluid exchange in the tube. Thus, the MLSs continuously disrupts the velocity boundary layer and consumes the kinetic energy of the mainstream flow, indicating that the heat transfer between the fluid and the wall is enhanced.

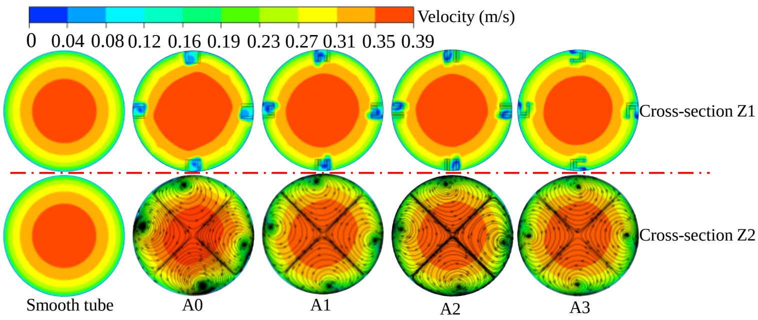

Figure 7. The velocity and streamlines distributions (*Re*=14000)

Fig. 8 shows the temperature distribution on cross-section Z2 for *Re* = 14000. The comparison reveals that the temperature field exhibits a similar distribution to the velocity field, with MLSs enhances the fluid disturbance and promotes the exchange of cold and hot fluids between the wall region and the center region. This indicates that as the temperature distribution becomes more uniform, the flow boundary layer and thermal boundary layer become thinner. The MLSs directly influence the temperature field distribution, while the thickness of the thermal boundary directly affects the convective heat transfer coefficient. The slotted structure weakens the intensity of the MLSs generated in the wall region, thereby weakening its disturbance effect on the thermal boundary layer, and resulting in decreased heat transfer efficiency.

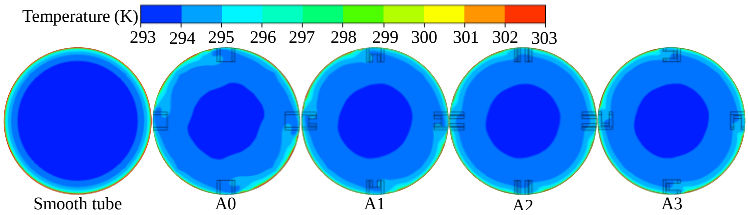

Figure 8. Temperature distributions (*Re* = 14000)

3.1.2 Thermohydraulic performance

Fig. 9(a) shows the effect of slotted structure on *Nu*. Compared with the smooth tube, the various structures of vortex generators increase the *Nu* in the tube. For the same *Re* condition, the A0 vortex generator exhibits a higher *Nu* than the other slotted structures, attributed to the greater destroy on the boundary layer induced by the A0 structure generated MLSs (Fig. 5 and Fig. 6), thus yielding the best heat transfer capacity. Fig. 9(b) shows the effect of slotted structure on f. The vortex generator improves the heat transfer but also causes pressure loss, indicating an increased flow resistance. It is usually considered that form resistance is the primary cause of pressure loss, and the A0 vortex generator possesses the larger upstream area than the three other slotted structures, leading to the largest increase in flow resistance. Furthermore, the A2 structure has the smaller header area than the A3 structure, while f is almost the same, suggesting that the fluid creates disturbance that affecting the intensity of the MLSs generation. Fig. 9(c) shows the effect of slotted structure on PEC. The utilization of the vortex generator improves the heat transfer capacity at the expense of increased flow losses, with all PEC values are all greater than 1 indicating that the heat transfer capacity increase surpasses the flow resistance increase. Comparison reveals that the A0 structure exhibits the best overall performance, confirming that both the fluid disturbance mechanism and the disturbance intensity have an impact on MLSs generation, which in turn affects the heat transfer capacity and pressure loss. Therefore, MLSs is an outstanding flow field structure, and promoting the generation of MLSs is crucial for improving the overall performance of tube.

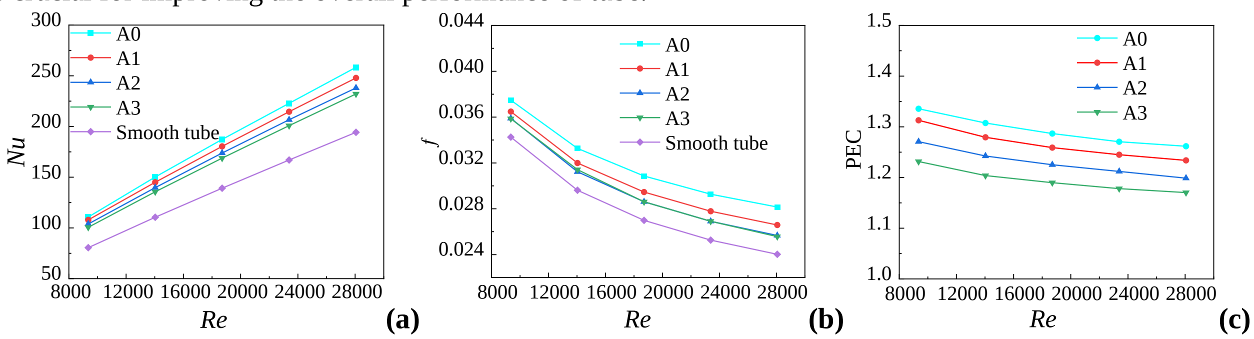

Figure 9. Effects of slotted structure: (a) *Nu*; (b) *f*; (c) PEC

3.2. Effect of longitudinal pitch on the thermohydraulic performance of rectangular vortex generator

Fig. 10 shows rectangular vortex generator tubes with three longitudinal pitch values (P = 0.1 m, 0.2

m and 0.3 m). To analyze the thermohydraulic performance of the tube, the cross-section at Z3=0.65 m is selected for the study.

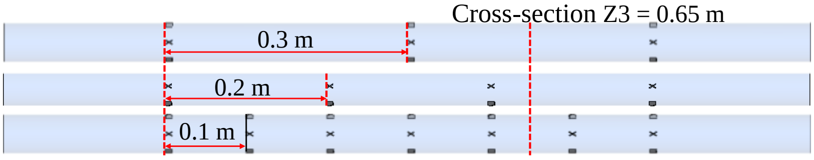

Figure 10. Different longitudinal pitch arrangement

3.2.1 Turbulent flow structures and thermal fields

The local streamlines at *Re* = 14000 is shown in Fig. 11. Observing the streamlines for the *P*=0.3 m, the vortex generator induces the fluid to generate swirls that do not develop consistently and their intensity diminishes with increasing pitch. With the *P* decreases, the disturbance to the fluid is more intense. At *P*=0.1, the disturbance is greater, and the swirls exhibit significant lateral expansion along the path length, which creates boundary layer disturbances.

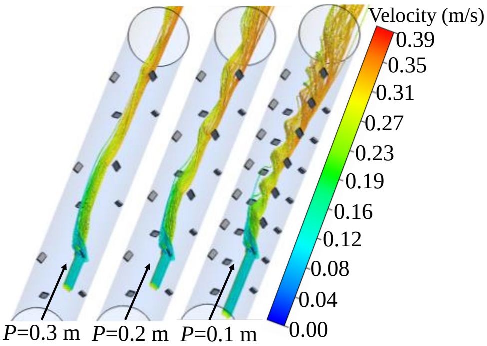

Figure 11. The local streamlines (*Re* = 14000)

The velocity and temperature distributions on cross-section Z3 for *Re* = 14000 are shown in Fig. 12. As observed from the velocity and temperature fields distribution, the MLSs accelerates the exchange of cold and hot fluids, effectively enhancing the heat transfer between the fluid and the wall. This heat transfer enhancement can be attributed to the disturbance of the thermal boundary layer. In the region of higher wall flow velocity, the thinner thermal boundary layer results in enhanced heat transfer. In contrary, the heat flow convergence is formed in the region of lower wall flow velocity accompanied by the thinner thermal boundary layer and smaller temperature gradient, which attenuates the heat transfer performance. The temperature distribution is more homogeneous for *P* = 0.1 m, with significantly more regions of thermal boundary layer thinning than thickening, which is also significantly higher than in the cases of *P* = 0.2 m and *P* = 0.3 m.

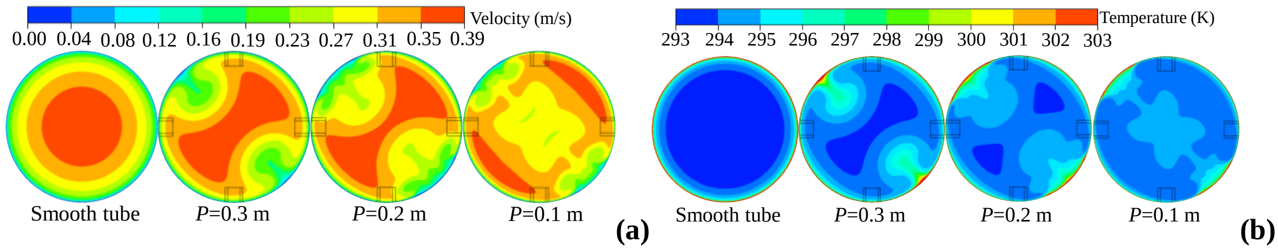

Figure 12. Velocity and temperature distributions on cross-section Z3 (*Re* = 14000): (a) velocity; (b) temperature

3.2.2 Thermohydraulic performance

The effect of longitudinal pitch of the rectangular vortex generator on *Nu*, *f* and PEC is shown in Fig. 13. The increase of *Nu* diminishes as *P* decreases, indicating graduall enhancement of heat transfer in the tube. This is attributed to the stronger destruction of the thermal boundary by the MLSs (Fig. 12). Moreover, the higher number of vortex generators obstruct the fluid, increasing *f*. From the evaluation of the PEC performance, the sacrifice of larger mainstream kinetic energy for *P* = 0.1 m results in PEC values ranging from 1.30 to 1.44, further verifying the generation of MLSs as the key to improving the overall performance of the tube.

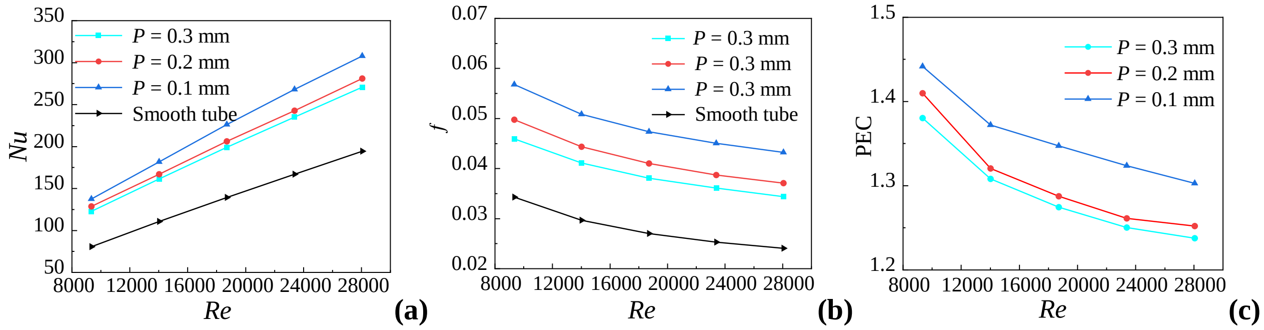

Figure 13. Effects of longitudinal pitch: (a) *Nu*; (b) *f*; (c) PEC

3.3. Comparison with previous work

Fig. 14 gives the comparison with the previous work with the PEC values. In this work, the rectangular vortex generator calculated has the best overall performance for *P* = 0.1 m. The PEC of the rectangular vortex generator is significantly better than those of delta-winglet pairs [17], winglet vortex generators [14], inclined vortex rings [13], multiple rectangular winglet [15] and spaced quadruple twisted tape [16], which indicates that the rectangular vortex generator can effectively improve the overall performance of the tube. Moreover, the PEC of the rectangular vortex generator is lower than those of coiled-wire inserts [19] and V-baffled tapes [18]. Therefore, the rectangular vortex generator provides the reference for heat exchanger tube design and industrial application.

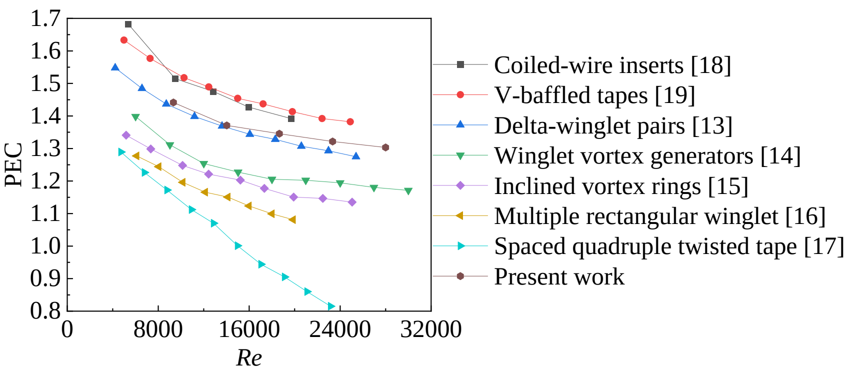

Figure 14. Comparison with previous work with PEC

4. Conclusion

This work compares the thermohydraulic performance of rectangular vortex generators and three slotted structures in the tube, as well as the effect of longitudinal pitch of rectangular vortex generators on *Nu*, *f* and PEC. The main conclusions are as follows:

- The fluid downstream of the spoiler element generates the swirls, and MLSs is generated in the heat exchanger tube. This accelerates the convergence of cold and hot fluids, improves the field synergy in the tube, and increases the heat transfer efficiency while causing pressure loss.

- Compared with the rectangular vortex generator, the slotted structure reduces the intensity of the MLSs and has the stronger effect on the fluid. The quantitative analysis results indicate that the rectangular vortex generator has the best overall performance, suggesting that the intensity of the MLSs directly affects the overall performance of the tube.
- With the decrease of the longitudinal pitch of the rectangular vortex generator, *Nu*, *f*, and PEC increase, and the tube exhibits better overall performance for the longitudinal pitch P = 0.1 m.
- In comparison with previous work, the vortex generator has excellent overall performance due to its ability to generate MLSs. Furthermore, more geometrical parameters require investigation and optimization in future work in order to improve the overall performance of the tube with vortex generator.

Nomenclature

C_p – specific heat capacity [$\mathrm{Jkg^{-1}K^{-1}}$]
D – inner diameter of the tube, [m]
f – friction coefficient
f_0 – friction factor of smooth tube
h – heat transfer coefficient [$\mathrm{Wm^{-2}K^{-1}}$]
k – thermal conductivity coefficient, [$\mathrm{Wm^{-1}K^{-1}}$]
L – length of the vortex generators [m]
H – height of the vortex generators [m]
Nu – Nusselt number
Nu_0 – Nusselt number of smooth tube
Δp – pressure drop of the test section, [Pa]
P – rib pitch, [mm]
Pr – Prandtl number
q – heat flux, [$\mathrm{Wm^{-2}}$]
Re – Reynolds number
T – temperature, [K]
T_w – average temperature of the tube wall, [K]
T_m – fluid mean temperature, [K]
u_m – average velocity, [$\mathrm{ms^{-1}}$]
W – width of the vortex generators [m]

Greek symbols

β – the attack angle [°]
μ – dynamic viscosity, [Pas]
ρ – fluid density, [$\mathrm{kgm^{-3}}$]

Acronyms

PEC – performance evaluation criteria
A0 – rectangular vortex generator
A1, A2, A3 – three different slotted structure

Acknowledgments

This work was supported by the Henan Provincial Department of Science and Technology Research Project (232102321086, 232102321091, 232102321087).

References

[1] Wang, Y. J., *et al*., Effect of Shell on Performance of Heat Exchanger with Trefoil-Hole Baffle, *Thermal Science, 26* (2022), 6B, pp. 4897-4907.
[2] Zheng, N. B., *et al*., A Review on Single-Phase Convective Heat Transfer Enhancement Based on Multi-Longitudinal Vortices in Heat Exchanger Tubes, *Applied Thermal Engineering, 164* (2020), Oct., 114475.
[3] Ekrani, S. M., *et al*., Multi-Objective Optimization of a Tubular Heat Exchanger Enhanced With Delta Winglet Vortex Generator and Nanofluid Using a Hybrid CFD-SVR Method, *International Journal of Thermal Sciences*, *186* (2023), Jan., 108141.
[4] Meng, J. A., *et al*., Field Synergy Optimization and Enhanced Heat Transfer by Multi-Longitudinal Vortexes Flow in Tube, *International Journal of Heat and Mass Transfer, 48* (2005), Apr., pp.

3331-3337.
[5] Khaboshan, H. N., *et al*., The Effect of Multi-Longitudinal Vortex Generation on Turbulent Convective Heat Transfer Within Alternating Elliptical Axis Tubes with Various Alternative Angles, *Case Studies in Thermal Engineering, 12* (2018), Apr., pp. 237-247.
[6] Wang, Y. J., *et al*., Design and Optimization on Symmetrical Wing Longitudinal Swirl Generators in Circular Tube for Laminar Flow, *International Journal of Heat and Mass Transfer, 193* (2022), Apr., 122961.
[7] Batule, P., *et al*., Heat Transfer and Pressure Drop Performance Improvement Using Curved Circular Spines for Flow Through Circular Pipe, *Thermal Science and Engineering Progress, 42* (2023), May, 101884.
[8] Xiao, H., *et al*., Turbulent Heat Transfer Enhancement in the Mini-Channel by Enhancing the Original Flow Pattern with V-Ribs, *International Journal of Heat and Mass Transfer, 163* (2020), Sept., 120378.
[9] Liu, P., *et al*., Heat Transfer Enhancement for Laminar Flow in a Tube Using Bidirectional Conical Strip Inserts, *International Journal of Heat and Mass Transfer, 127* (2018), Sept., pp. 1064-1076.
[10] Lv, J. Y., *et al*., Active Design for the Tube Insert of Center-Connected Deflectors Based on the Principle of Exergy Destruction Minimization, *International Journal of Heat and Mass Transfer, 150* (2020), Jan., 119260.
[11] Ali, S., *et al*., Three-Dimensional Numerical Study of Heat Transfer and Mixing Enhancement in a Circular Pipe Using Self-Sustained Oscillating Flexible Vorticity Generators, *Chemical Engineering Science, 162* (2017), Dec., pp. 152-174.
[12] Mohammed, H. A., *et al*., Heat Transfer Augmentation of Parabolic Trough Solar Collector Receiver's Tube Using Hybrid Nanofluids and Conical Turbulators, *Journal of the Taiwan Institute of Chemical Engineers, 125* (2021), Jul., pp. 215-242.
[13] Promvonge, P., *et al*., Thermal Performance Enhancement in a Heat Exchanger Tube Fitted With Inclined Vortex Rings, *Applied Thermal Engineering, 62* (2014), *et al*., pp. 285-292.
[14] Xu,Y., *et al*., Experimental Study of Thermal Performance and Flow Behaviour With Winglet Vortex Generators in a Circular Tube, *Applied Thermal Engineering, 135* (2018), Jan., pp. 257-268.
[15] Sun, Z. Q., *et al*., Investigations of The Turbulent Thermal-Hydraulic Performance in Circular Heat Exchanger Tubes With Multiple Rectangular Winglet Vortex Generators, *Applied Thermal Engineering, 168* (2020), Dec., 114838.
[16] Samruaisin, P., *et al*., Influence of Regularly Spaced Quadruple Twisted Tape Elements on Thermal Enhancement Characteristics, *Chemical Engineering and Processing-Process Intensification, 128* (2018), Apr., pp. 114-123.
[17] Koolnapadol, N., *et al*., Effect of Pitch Spring of Delta-Winglets on Thermal Characteristics in a Heat Exchanger Tube, *Journal of Research and Applications in Mechanical Engineering, 4* (2016), 2, pp. 1-9.
[18] Promvonge, P., Skullong, S., Augmented Heat Transfer in Tubular Heat Exchanger Fitted with V-Baffled Tapes, *International Journal of Thermal Sciences, 155* (2020), May, 106429.
[19] Keklikcioglu, O., Ozceyhan, V., Experimental Investigation on Heat Transfer Enhancement of a Tube with Coiled-Wire Inserts Installed with a Separation From the Tube Wall, *International Communications in Heat and Mass Transfer, 78* (2016), Sept., pp. 88-94.

Submitted: 27.11.2023
Revised: 12.01.2024
Accepted: 25.01.2024